J Appl Electrochem (2007) 37:759–764
DOI 10.1007/s10800-007-9311-7

ORIGINAL PAPER

Effects of mechanical grinding on initial activation and rate capability of Zr–Ti based Laves phase alloy electrode

Masao Matsuoka · Kazuaki Tamura

Received: 22 November 2006 / Accepted: 9 February 2007 / Published online: 7 March 2007

Abstract Surface modification of $Zr_{0.9}Ti_{0.1}Ni_{1.1}Co_{0.1}Mn_{0.5}V_{0.2}Cr_{0.1}$ alloy was accomplished by mechanical grinding (MG). The decrepitation of alloy particles gave rise to a new surface. The effect of MG was systematically studied by X-ray diffraction (XRD), scanning electron microscopy (SEM), pressure-composition (PC) isotherms and electrochemical impedance spectroscopy (EIS). Initial activation and rate capability of a negative electrode made from this alloy were significantly improved by MG treatment at 300 rpm for 0.5–1 h, but prolonged MG treatment (10 h) reduced the nominal discharge capacity from 350 mAh g^{-1} to 180 mAh g^{-1}. Under these conditions the alloy particles disintegrate and become nanocrystalline, which reduces the discharge capacity owing to the change in the stereology of tetrahedral interstices available for hydrogen storage. The data based on PC isotherms and hydriding kinetics indicates that the equilibrium hydrogen pressure increases and the hydriding rate and storage capacity are significantly reduced by prolonged MG treatment. EIS data reveal that the improved rate capability can be ascribed to an enhanced charge-transfer reaction which is the rate-determining step in the hydriding and dehydriding reactions.

Keywords Laves phase alloy · MH battery · Hydriding kinetics · Mechanical grinding · Lattice strain

M. Matsuoka (✉) · K. Tamura
Department of Applied Chemistry, Faculty of Science and Engineering, Ritsumeikan University, Nojihigashi, Kusatsu, Shiga 525-8577, Japan
e-mail: matsuoka@se.ritsumei.ac.jp

1 Introduction

Nickel-hydride (MH) batteries that use a hydrogen storage alloy as a negative electrode material are characterized by high energy density, 1.5–2 times that of Ni-Cd batteries, in addition to environmental compatibility. Since 1989, MH batteries using a rare earth-based AB_5 type alloy have been widely employed as power sources in electronic appliances and small portable devices for non-military use. Recent trends in the use of MH batteries have been in applications such as in the field of hybrid electric vehicles and electromechanical tools, where high power and high capacity are necessary. In order to achieve further high capacity and power density, new hydrogen storage alloys based on the rare earth-magnesium-nickel system have been intensively investigated [1–3]. At present, a superlattice alloy based on rare earth-magnesium is employed as a negative electrode material and, in an AA size MH battery, can achieve a capacity of 2,500 mAh [4]. Laves phase AB_2 alloy [5–7] is also a potential candidate to further improve the energy density of MH batteries. However, practical use of Laves phase alloy is restricted by slow activation and insufficient rate capability, due to the presence of a passive film on the surface and slow hydrogen diffusivity in the alloy. Rapid activation of hydrogen storage alloys is essential for practical applications; therefore, many approaches such as anodic oxidation [8], alkaline treatment at elevated temperature [9–11] and HF treatment [12, 13] have been successfully carried out. In addition, physical modification of the surface with the aid of ball milling has been found to be effective for initial activation of alloys. Sun et al. [14]. revealed that ball milling of Zr–Cr–Ni based alloy with Ni powder improves the initial activation when used as a negative electrode. Lee et al. [15] improved the kinetic properties

of a Zr-based negative electrode by mechanical grinding (MG) using a surface modifying powder of Ti-based alloy.

In this study the effect of MG on the performance of a Zr–Ti based hydrogen storage alloy negative electrode was investigated, because the decrepitation rate is very sensitive to the brittleness of the alloy. During the MG treatment decrepitation creates a new and fresh surface increases the effective surface area and also changes the crystallinity and lattice strain. The effects of MG treatment on the performance and kinetic parameters of the negative electrode were evaluated using galvanostatic charge-discharge cycles and electrochemical impedance spectroscopy (EIS). The changes in the performance of the negative electrode are discussed from the viewpoint of crystal structure, BET surface area, kinetics of the hydrogen electrode reaction, pressure-composition (PC) isotherms and hydriding kinetics of alloy particles.

2 Experimental

2.1 Electrode preparation and electrochemical measurements

Hydrogen storage AB_2 alloy with a composition of $Zr_{0.9}Ti_{0.1}Ni_{1.1}Co_{0.1}Mn_{0.5}V_{0.2}Cr_{0.1}$ was prepared by induction melting and pulverized to less than 100 μm for use as a standard sample. This alloy was supplied as a common sample from Osaka National Research Institute and was used to standardize the characterization method of hydrogen storage alloys. The alloy powder (1 g) was placed in a stainless steel pot (45 cm^3) together with 10 balls (ϕ 10 mm) under an Ar atmosphere and MG treatment was carried out using a planetary ball mill (Fritsch Pulverisette 7) at a rotation speed of 300 rpm for 0.5–10 h. Negative electrodes (ϕ10 mm) were constructed by pressing a mixture of alloy (0.1 g) and electrolytic copper (0.3 g) powders under a pressure of 10 ton cm^{-2} and nickel mesh and wire as a current collector were then firmly attached by spot welding.

Electrochemical cycling was performed at 298 K using a computer-assisted charge-discharge unit (Hokuto Denko, HJ101SM6). The negative electrode was mounted in the central part of a three-compartment Pyrex cell containing de-aerated 6 M KOH solution and two positive NiOOH electrodes on both sides. After charging 500 mAh g^{-1} at a current density of 100 mA g^{-1}, the circuit was opened for 30 min, and then discharged at 40 mA g^{-1} to a cut off potential of –0.6 V versus the Hg/HgO/6 M KOH reference electrode. The rate capability, defined by the following equation, was evaluated by changing the discharge current density from 80 to 480 mA g^{-1}.

$$R_c(i) = C(i)/C(40) \times 100\%$$

where, $R_c(i)$ is the rate capability at i mA g^{-1}, and $C(i)$ and $C(40)$ are discharge capacities measured at a discharge current density of i and 40 mA g^{-1}, respectively.

For the EIS measurement a frequency response analyzer (NF Electronic Inst., 5080 type) equipped with a potentiostat/galvanostat (Hokuto Denko, HA-501G) was operated in the frequency range 0.01 Hz–20 kHz with an amplitude of 10 mV. The impedance spectra of the modified electrodes were measured at 298 K under equilibrium potential after fully charging at the 1st cycle. In the case of an unmodified electrode the measurement was carried out at the 1st and 20th cycle after fully charging.

2.2 Characterization of alloy powders

The morphology and crystallographic feature were characterized using a scanning electron microscope (SEM; Hitachi, S-2460N) and X-ray diffraction (XRD; Rigaku, RINT2000). The analysis of the XRD peaks was carried out by the Williamson-Hall method. The crystallite size (d) and lattice strain (ε) were determined according to the following equation [16].

$$(\beta_e^2 - \beta_i{}^2)^{1/2} \cos\theta/\lambda = 0.9/d + 2\varepsilon \sin\theta/\lambda \quad (1)$$

where, λ is the wavelength of Cu Ka radiation (0.15405 nm), β_e is the full-width at half-maximum of the diffraction peak in radian, and β_i is the instrumental broadening, which was determined using the standard Si powder.

The specific surface area of alloy particles was determined by the Brunauer, Emmett and Teller (BET) method using a Belsorp-min (Bel Japan, Inc.). Sieverts-type equipment (Lesca, PCT-A10B) was used to measure PC isotherms for hydriding and dehydriding at 298 K and also to determine the absorption rate of hydrogen by measuring the pressure change after introduction of hydrogen at 3 MPa into a sample tube containing alloy powder dehydrided in vacuum at 523 K.

3 Results and discussion

3.1 Particle size and BET surface area

The particle size, determined by SEM observation, and the surface area evaluated by the BET method are shown in Fig. 1 as a function of MG grinding time. The specific surface area of $Zr_{0.9}Ti_{0.1}Ni_{1.1}Co_{0.1}Mn_{0.5}$ $V_{0.2}Cr_{0.1}$ alloy was significantly increased by MG treatment during the

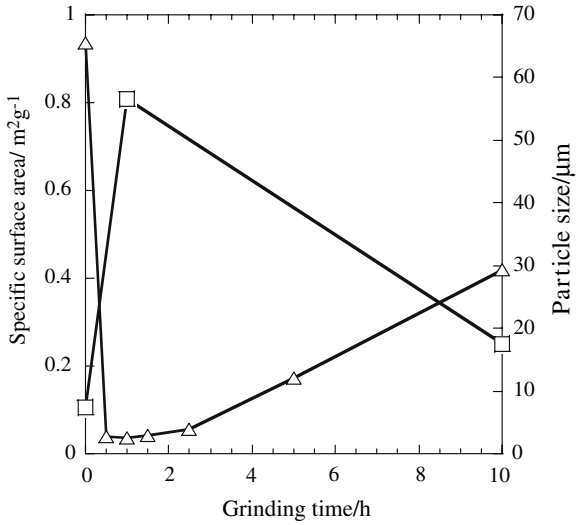

Fig. 1 Changes in the specific surface area and size of alloy particles with grinding time

first 1 h, and was at a maximum (0.8 m^2 g^{-1}) at 1 h, but then decreased to 0.25 m^2 g^{-1} after 10 h of MG treatment. The particle size of the alloys was found to decrease from 65 μm to a minimum of 2 μm at approximately 1 h of MG treatment, and then increased to 30 μm after 10 h. Consequently, a minimum particle size and a maximum specific surface could be achieved by MG treatment for 1 h, because the generation of a new surface by decrepitation was followed by the coagulation of primary particles due to cold welding during prolonged MG treatment. The same phenomena was reported by Ikeya et al. for a mixture of mishmetal-system alloy and 20 wt.% Co powders [17]; however, the incubation time required to yield a maximum surface area and starting time of coagulation was much longer than that in the present study. It is presumed that this depends on the equipment used for the MG treatment and the presence of a modifier.

3.2 Crystal structure and hydriding kinetics

Typical XRD profiles of $Zr_{0.9}Ti_{0.1}Ni_{1.1}Co_{0.1}Mn_{0.5}$ $V_{0.2}Cr_{0.1}$ alloy are shown in Fig. 2. The diffraction lines of the unmodified sample, shown in Fig. 2(a), were assigned to the cubic C15 Laves phase structure. However, the diffraction intensity decreased and broadened with increasing MG treatment time. In particular, diffraction peaks with higher Miller indices were hardly detected after 5 h of MG treatment. This indicates that the mechanical impact during the grinding gives rise to a nanocrystalline structure with a high lattice strain. According to Burgio et al. [18], it was pointed out that nanostructuring was followed by amorphization with increasing rotation velocity and milling time in the Fe-Zr system. However, nanostructuring was mainly recognized in our experimental conditions because the power of Pulverisette 7 was smaller than that of Pulverisett 5 used in [18].

The broadening of diffraction peaks was analyzed using the Williamson-Hall method. The results are shown in Fig. 3. According to Eq. 1, the plots of $(\beta_e^2-\beta_i^2)^{1/2}\cos\theta/\lambda$ against $2\sin\theta/\lambda$ give a straight line. The lattice strain, which was calculated using the slope of the straight line, increased with increasing the MG time, giving the values of 0.1% (0 h), 0.31% (0.5 h), 0.45% (1 h), 0.70% (2.5 h), 0.92% (5 h), and 1.01% (10 h). The crystallite size evaluated from the y-intercept of the line was found to be 778 nm (0 h), 95 nm (0.5 h), 98 nm (1 h), 69 nm (2.5 h), 17 nm (5 h), and 14 nm (10 h). The crystallite size decreased and lattice strain increased with elapsed MG time, reaching a limiting value when the milling became longer than 5 h. As a result the stereology of the tetrahedral interstices in the cubic lattice, used for hydrogen storage, would be significantly changed by prolonged grinding.

PC isotherms of the alloys, which had undergone MG treatment for 0–10 h at 300 rpm, were measured at 298 K and are shown in Fig. 4. The PC isotherms shifted to a lower hydrogen-to-metal ratio (H/M) with increase in grinding time. Hydrogen storage capacities were calculated from the H/M values at a hydrogen pressure of 0.1 MPa, and were 410, 344 and 240 mAh g^{-1} for the samples ground for 0 h, 1 h and 10 h, respectively. This significant decrease in capacity can be ascribed to the changes in the stereology of the tetrahedral interstices in the cubic lattice. According to Ivey et al. [19], there are 16 tetrahedral interstices available for hydrogen storage (four 32e sites consisting of 1A and 3B atoms, and twelve 96 g sites consisting of 2A and 2B atoms) in the AB_2 Laves phase alloy with C15 structure, but the maximum number of hydrogen atoms per formula unit is restricted to 6 due to electrostatic limitations. The calculated hydrogen storage capacity of 410 mAh g^{-1} corresponds to three hydrogen atoms per AB_2 formula.

The results of the hydriding rate measured at 298 K are shown in Fig. 5. For the unmodified sample the hydriding rate was quite rapid and a high hydrogen storage capacity (H/M = 1.05) was achieved immediately after introduction of the hydrogen gas. However, the hydriding rate and hydrogen storage capacity of the mechanically ground samples decreased with increase in grinding time. Because the stereology of the tetrahedral interstices available for hydrogen storage are changed by grinding absorbed hydrogen must be present as a solid solution without hydride formation, which gives rise to a slow hydriding rate and low hydrogen storage capacity. Kirchheim [20] reported that the diffusivity of hydrogen in strained Pd or Pd-based amorphous alloys was significantly reduced with decrease in the hydrogen concentration, due to the

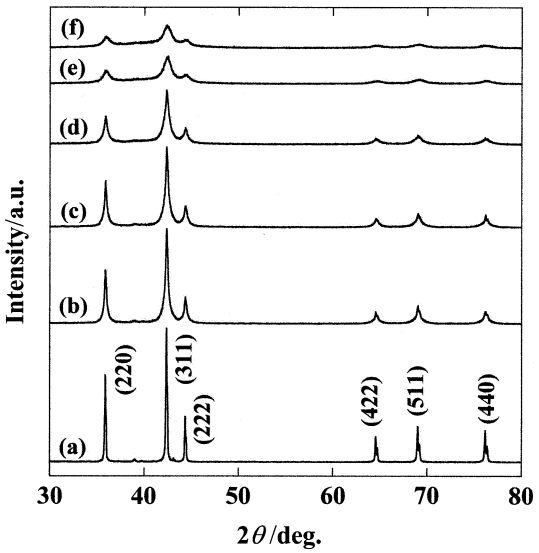

Fig. 2 X-ray diffraction profiles of Zr–Ti based alloy as a function of grinding time. (a) 0 h, (b) 0.5 h, (c) 1 h, (d) 2.5 h, (e) 5 h, (f) 10 h

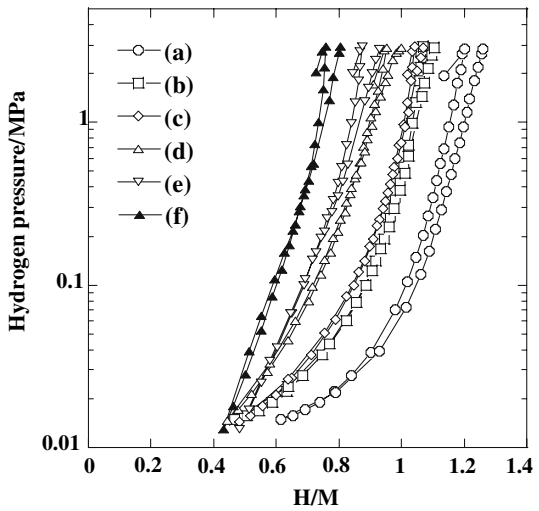

Fig. 4 PC isotherms for the Zr–Ti based alloy-hydrogen system as a function of grinding time. (a) 0 h, (b) 0.5 h, (c) 1 h, (d) 2.5 h, (e) 5 h, (f) 10 h

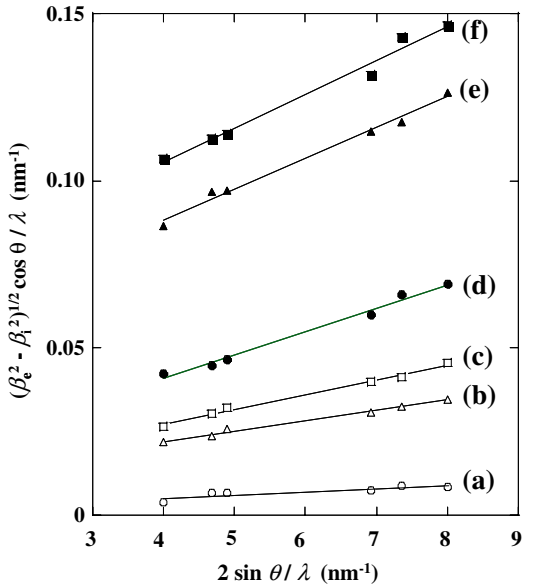

Fig. 3 Williamson-Hall plot for Zr–Ti based hydrogen storage alloys as a function of grinding time. (a) 0 h, (b) 0.5 h, (c) 1 h, (d) 2.5 h, (e) 5 h, (f) 10 h

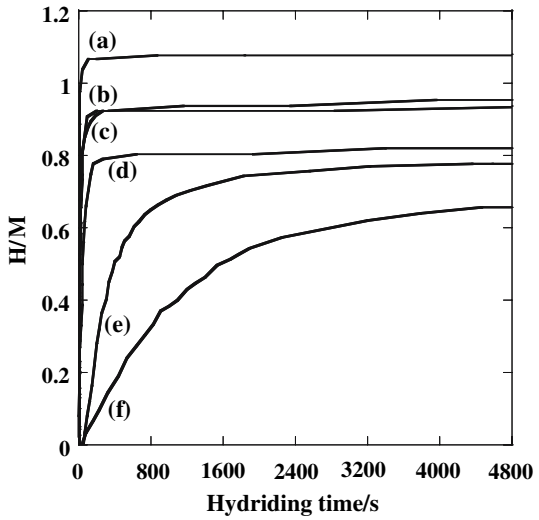

Fig. 5 Hydriding kinetics of Zr–Ti based hydrogen storage alloy as a function of grinding time. (a) 0 h, (b) 0.5 h, (c) 1 h, (d) 2.5 h, (e) 5 h, (f) 10 h

appearance of energetically stable hydrogen trapping sites. Consequently, the stress induced by prolonged MG treatment also depressed the hydriding kinetics.

3.3 Discharge capacity and rate capability

The cyclic discharge capacities of the negative electrodes measured at 298 K are shown in Fig. 6 as a function of the mechanical grinding time. The discharge capacity of unmodified $Zr_{0.9}Ti_{0.1}Ni_{1.1}Co_{0.1}Mn_{0.5}$ $V_{0.2}Cr_{0.1}$ alloy gradually increased with the number of charge and discharge cycles; however, more than 20 cycles was required for complete activation. For the samples that had undergone MG treatment for 0.5–1 h, higher discharge capacity and rapid activation were obtained compared to that of the unmodified sample. The best result was obtained for a 1 h MG treatment, which resulted in a nominal discharge capacity (350 mAh g^{-1}) from the 5th cycle. This capacity is comparable to the value calculated from PC isotherms. Although the PC isotherms indicated that higher capacity was expected for unmodified Zr–Ti alloy, some existing tetrahedral sites were not available for hydrogen storage

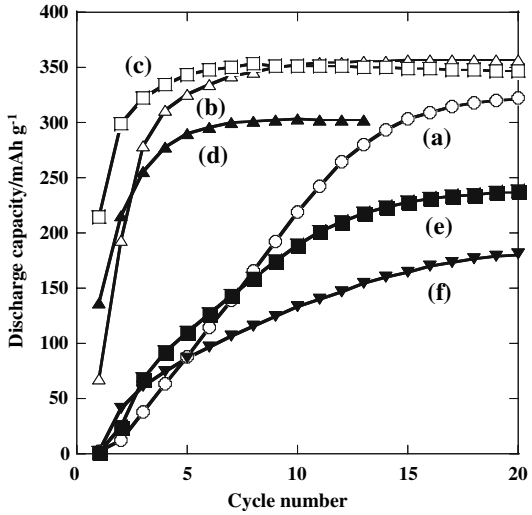

Fig. 6 Discharge capacity of Zr–Ti based alloy electrodes as a function of grinding time. (a) 0 h, (b) 0.5 h, (c) 1 h, (d) 2.5 h, (e) 5 h, (f) 10 h

because of the presence of an inactive oxide layer on the surface, which resulted in slow activation profile as shown by the curve (a) in Fig. 6. Therefore, this favorable effect of MG treatment reflects the generation of a new active surface without damage to the sample crystallinity. However, for the case of prolonged MG from 5 to 10 h the attainable discharge capacity significantly decreased compared to the unmodified sample because of the changes in the stereology of tetrahedral interstices available for hydrogen storage.

The effect of grinding time on the rate capability of $Zr_{0.9}Ti_{0.1}Ni_{1.1}Co_{0.1}Mn_{0.5}V_{0.2}Cr_{0.1}$ alloy electrodes is shown in Fig. 7. A distinct increase in the rate capability was observed after MG treatment for up to 1 h. The best result was obtained for the sample ground for 1 h and the rate capability was found to be 60% even at a discharge current density of 480 mA g^{-1}. Further increase in the grinding time resulted in a significant decrease in the rate capability. For example, the performance of the sample that was ground for 10 h became lower than that of the unmodified sample.

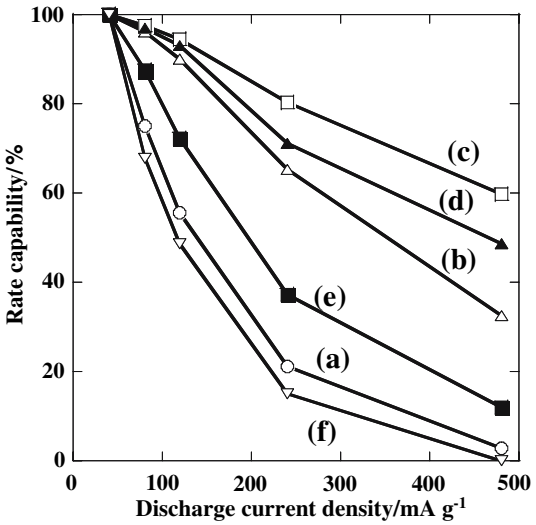

Fig. 7 Rate capability of Zr–Ti based alloy electrodes as a function of grinding time at 300 rpm. (a) 0 h, (b) 0.5 h, (c) 1 h, (d) 2.5 h, (e) 5 h, (f) 10 h

3.4 Charge transfer reaction

The kinetic parameter of the hydrogen electrode reaction was evaluated using EIS for the electrodes at full charge and at equilibrium potential. Nyquist plots as a function of the charge and discharge cycle and grinding time are shown in Fig. 8. For all Nyquist plots measured at equilibrium potential after fully charging Warburg impedance could not be detected; therefore, it was concluded that the rate-determining step is the charge transfer reaction. In the case of the unmodified electrode a large semicircle was detected at the 1st cycle, as indicated by curve (a), indicating a charge transfer resistance of ca.75 Ω (3.4 mA g^{-1}). The value in parenthesis indicates the corresponding exchange current density. However, the charge transfer resistance decreased to 15 Ω (17.1 mA g^{-1}) after repeating 20 charge and discharge cycles, as indicated by curve (d). For the samples ground for 1 h and 2.5 h, indicated by curves (b) and (c), the resistance was found to be 12 Ω (21.4 mA g^{-1}) and 17 Ω (15.1 mA g^{-1}), respectively, even at the 1st cycle. These resistance values are comparable to that of an activated negative electrode consisting of unmodified alloys. Further increase in the grinding time, up to 10 h, resulted in an increase in the resistance to 25 Ω (10.3 mA g^{-1}), as indicated by curve (e). This indicates that short-time grinding is beneficial but prolonged grinding produces an unfavorable effect against the charge transfer reaction of hydrogen.

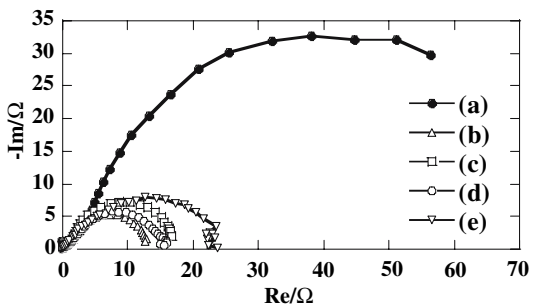

Fig. 8 Nyquist plots of a MG-treated Zr–Ti based alloy electrode at the 1st cycle and an unmodified electrode at the 1st and 20th cycles under a fully charged condition. (a) 0 h-MG/1st, (b) 1 h-MG/1st, (c) 2.5 h-MG/1st, (d) 0 h-MG/20th, (e) 10 h-MG/1st

Therefore, the rate capability is exclusively improved by a shortened diffusion path, which increases the flux of hydrogen and by an increased effective surface area which substantially reduces the real current density.

4 Conclusions

The effects of mechanical grinding on the performance of Zr–Ti based alloy as a negative electrode material were evaluated by electrochemical techniques and changes in kinetic parameters were discussed on the basis of physicochemical data obtained by XRD, SEM and BET isotherms. The following results were obtained.

1. Mechanical grinding of the $Zr_{0.9}Ti_{0.1}Ni_{1.1}$-$Co_{0.1}Mn_{0.5}V_{0.2}Cr_{0.1}$ alloy at 300 rpm under an Ar atmosphere gives rise to crystallographic and morphological changes. Maximum BET surface area and minimum particle size are obtained by mechanical grinding for 1 h.
2. The best result for initial activation and high rate capability was obtained by mechanical grinding for 1 h. The unmodified sample requires more than 20 activation cycles, but this was shortened to a few cycles in order to achieve a nominal discharge capacity of 350 mAh g^{-1}.
3. EIS analysis indicates that activation by electrochemical cycling and mechanical grinding is characterized by a decrease in the charge transfer resistance.
4. Prolonged mechanical grinding caused a drastic decrease in the discharge capacity, because of the changes in the stereology of tetrahedral interstices available for hydrogen storage.
5. An improved high rate capability of the $Zr_{0.9}Ti_{0.1}Ni_{1.1}$-$Co_{0.1}Mn_{0.5}V_{0.2}Cr_{0.1}$ alloy electrode was correlated to an increased effective surface area and a shortened diffusion path for hydrogen.

References

1. Kohno T, Yoshida H, Kawashima F, Inaba T, Sakai I, Yamamoto M, Kanda M (2000) J Alloys Comp 311:L5–L7
2. Liu Y, Pan H, Gao M, Zhu Y, Lei Y, Wang Q (2004) Int J Hydrogen Energy 29:297–305
3. Wang Y, Gao XP, Lu ZW, Hu WK, Zhou Z, Qu JQ, Shen PW (2005) Electrochim Acta 50:2187–2191
4. Yasuoka S, Magari Y, Murata T, Tanaka T, Ishida J, Nakamura H, Nohma T, Kihara M, Baba Y, Teraoka H (2006) J Power Sources 156:662–666
5. Fetcenko MA, Venkatesan S (1990) Prog Batter Sol Cells 9:259–264
6. Moriwaki Y, Gamo T, Shintani A, Iwaki T (1989) Denki Kagaku 57:488–491
7. Sawa H, Wakao S, Furukawa J (1990) Denki Kagaku 58:862–867
8. Wakao S, Sawa H, Furukawa J (1991) Denki Kagaku 59:945–949
9. Zuttel A, Mail F, Schlapbach L (1994) J Alloys Compd 209:99–105
10. Yan D, Sandrock G, Suda S (1994) J Alloys Compd 216:237–242
11. Iwakura C, Choi WK, Zhang SG, Inoue H (1999) Electrochim Acta 44:1677–1679
12. Gao XP, Zhang W, Yang HB, Song DY, Zhang YS, Zhou ZX, Shen PW (1996) J Alloys Compd 235:225–231
13. Li ZP, Higuchi E, Liu BH, Suda S (1999) J Alloys Compd 293–295:593–600
14. Sun D, Latroche M, Percheron-Guegan A (1997) J Alloys Compd 257:302–305
15. Lee S-M, Kim S-H, Lee J-Y (2002) J Alloys Compd 330–332:796–801
16. Hesabi ZR, Simchi A, Reihani SMS (2006) Mater Sci Eng A428:159–168
17. Ikeya T, Kumai K, Iwahori T (1993) J Electrochem Soc 140:3082–3086
18. Burgio N, Iasonna A, Magini M, Martelli S, Padella F (1991) Il Nuovo Cimento 13D:459–476
19. Ivey DG, Northwood DO (1986) Ziet Phys Chem NF 147:191–209
20. Kirchheim R (1982) Acta Metall 30:1069–1107